



Skin friction reduction characteristics of variable ovoid non-smooth surfaces*

Xiao-wen SONG[†], Peng-zhe LIN, Rui LIU, Pei ZHOU

(State Key Laboratory of Fluid Power and Mechatronics Systems, Zhejiang University, Hangzhou 310027, China)

[†]E-mail: songxw@zju.edu.cn

Received Dec. 6, 2015; Revision accepted June 2, 2016; Crosschecked Dec. 19, 2016

Abstract: The use of bionic non-smooth surfaces is a popular approach for saving energy because of their drag reduction property. Conventional non-smooth structures include riblets and dimples. Inspired by sand dunes, a novel variable ovoid non-smooth structure is proposed in this study. The body of the variable ovoid dimple was designed based on three size parameters, the radius, semimajor, and depth, and a 3D model was created based on UG software. The constructed variable dimples were placed in a rectangular array on the bottom of a square tube model. Following ANSYS meshing, the grid model was imported into FLUENT, where the flow characteristics were calculated. Results of skin friction reduction were achieved and the effect of the design parameters on different variable ovoid dimples was obtained by orthogonal testing. Various aspects of the skin friction reduction mechanism were discussed including the distribution of velocity vectors, variation in boundary layer thickness, and pressure distribution.

Key words: Variable ovoid dimple; Non-smooth surface; Numerical simulation; Skin friction reduction
<http://dx.doi.org/10.1631/jzus.A1500324>

CLC number: TH161.12

1 Introduction

Research on reducing the skin friction of surfaces by covering them with bionic non-smooth structures has provided a new method for saving energy. This work has attracted many researchers to conduct correlational studies. Bionic research on the surfaces of many animals shows that non-smooth structures can reduce frictional drag. The skin of sharks effectively reduces the frictional drag in a turbulent-flow regime (Dean and Bhushan, 2010), and the pelage of bats living in Western Australia achieves a 10% drag reduction in high-speed flight (Bullen and McKenzie, 2008). Soil animals universally have non-smooth surfaces which demonstrate exceptional anti-resistance properties (Ren, 2009).

Inspired by the drag reduction properties and morphological geometry of creatures' non-smooth surfaces, researchers have designed many non-smooth structures, like riblets and dimples, which can reduce frictional drag in water or air. Practical applications, such as riblets on aircraft (Viswanath, 2002) and on swim suits (Matthews, 2008), are used commercially. Dimples (Choi *et al.*, 2006) and riblets (Kim and Choi, 2014) on a golf ball cause a reduction in drag compared with a smooth golf ball. Studies on other non-smooth structures, such as dimples on rubber seals (Gu *et al.*, 2013), dimples on revolving bodies (Zhang *et al.*, 2008), and bionically inspired surfaces on motor vehicles (Song *et al.*, 2011), show the great potential for the application of non-smooth structures.

The shape of non-smooth structures varies greatly. Regular riblets have a simple symmetrical shape with a triangular, semi-circular or square (Bourisli and Al-Sahhaf, 2008), sawtooth, scalloped

* Project supported by the National Natural Science Foundation of China (No. 51375439)

 ORCID: Xiao-wen SONG, <http://orcid.org/0000-0001-6386-9836>
© Zhejiang University and Springer-Verlag Berlin Heidelberg 2017

or blade (Dean and Bhushan, 2012) cross section. A bionic shark scale is much more complex, having a shape almost identical to that of real scale through highly-accurate scanning and data processing (Zhang *et al.*, 2011). Compared with the variety of riblets, dimples are much simpler, having a circular cross-sectional shape. The barchan dune vortex generator has less drag and higher stability than a V-gutter at the same inflow rate (Gao and Huang, 1982). The shape of the variable ovoid dimple presented in this study was inspired by sand dunes, and the study involves an investigation of the reduction in skin friction achieved by a dune surface in a turbulent boundary layer. Experiments, such as water tunnel tests (Bixler and Bhushan, 2013) and air tunnel tests (Boiko *et al.*, 2007), have been used to study the flow characteristics of non-smooth surfaces. In this study, the reduction in skin friction achieved by a flat surface with variable ovoid dimples and its mechanism were studied by numerical simulation.

2 Numerical simulation preprocessing

2.1 Model extraction

The variable ovoid units are dimples inspired by sand dunes (Fig. 1), which are formed by the interaction of sand with the flow of air. Fig. 2 shows the cross section of an ovoid that is geometrically similar to a sand dune. There are two main differences between a sand dune and an ovoid: (1) the opening curve of a sand dune is irregular while that of an ovoid is oval; (2) the curve of the cross section of a sand dune is a horizontal tangent while that of an ovoid is a vertical tangent.



Fig. 1 Dune topography

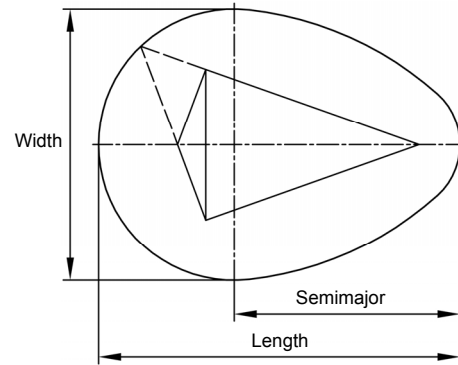


Fig. 2 Cross section of an ovoid

By combining the characteristics of a sand dune and an ovoid, a variable ovoid dimple is presented. The opening curve of the dimple is designed as a circle. The arc radius of the opening curve is expressed as r (Fig. 3c), so the equation of the opening curve can be defined as

$$x^2 + y^2 = r^2. \quad (1)$$

The curve of the longitudinal cross section of the variable ovoid dimple in Fig. 3a is drawn as a spline curve, which is similar to an ovoid but tangent to the horizon at both the left and right vertices.

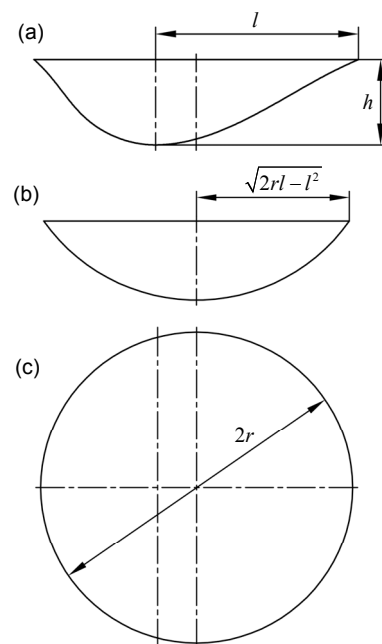


Fig. 3 Variable ovoid dimple

(a) Longitudinal cross section; (b) Transverse cross section; (c) Opening curve. l is the semimajor; h is the depth

The transverse cross section of the dimple is designed as an arc (Fig. 3b), where the curve equation is

$$y^2 + \left(z^2 + \frac{2rl - h^2 - l^2}{2h} \right)^2 = \left(\frac{h^2 - l^2 + 2rl}{2h} \right)^2. \quad (2)$$

By lifting the opening curve and the curves of both the longitudinal and transverse cross sections, the surface of a variable ovoid dimple was created using UG NX 8.5 (Fig. 4). Then the variable ovoid dimples were arranged in a rectangular array on the bottom of a square tube model (Fig. 5).

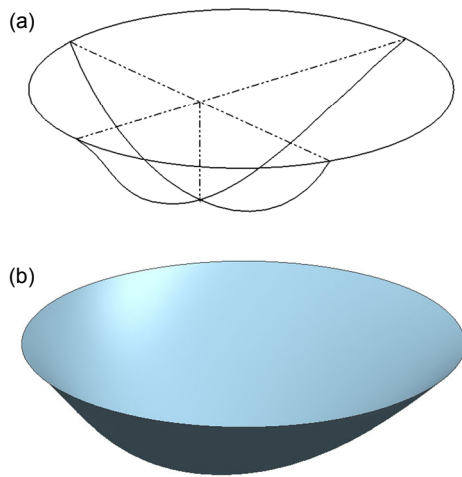


Fig. 4 Surface model
(a) Wireframe; (b) Shaded surface

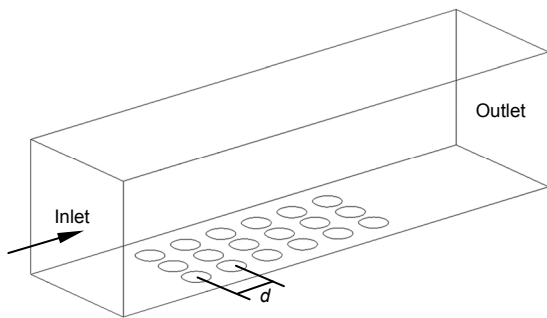


Fig. 5 Simulation model of a flat surface with variable ovoid dimples

It is found that if the dimensions of the non-smooth structure are small enough to be contained within the logarithmic law layer, the internal boundary layer will be changed effectively (Song *et al.*,

2011). Based on this phenomenon, three levels of dimensions of the variable ovoid dimple were set (Table 1).

Table 1 Level factors of the variable ovoid dimple

Level	Radius, r (mm)	Semimajor, l	Depth, h (mm)	Spacing, d (mm)
1	0.6	$1.25r$	0.2	2.0
2	0.7	$1.50r$	0.3	2.5
3	0.8	$0.50r$	0.4	3.0

2.2 Grid generation and initialization

The grid model of the square tube was generated as unstructured grids by ANSYS 14.5 Workbench Meshing. The size of the square tube model was $8\text{ mm} \times 8\text{ mm} \times 30\text{ mm}$. The grid size of the variable ovoid non-smooth surface was defined as 0.1 mm, and the other surfaces as 0.5 mm. The near-wall zone of the variable ovoid non-smooth surface was set on the bottom, with a transition area between the near-wall zone mesh and the surrounding mesh to satisfy the surface area calculation requirements. To meet the needs of the surface area calculation, an inflation layer was set on the surface. The grid model is shown in Fig. 6. The total number of cells was about 1.14×10^6 and their minimum and maximum volumes were 5.91×10^{-6} and 0.164 mm^3 , respectively.

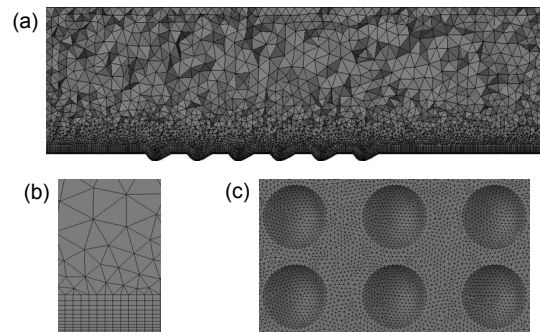


Fig. 6 Grid model of the square tube
(a) Whole grid; (b) Refinement layer; (c) Grid of the variable ovoid dimples

The grid model was then imported into FLUENT 14.5 for numerical simulation. In consideration of applications to automobiles and other ground vehicles, the fluid speed of the velocity inlet ranged from 8 to 24 m/s. Initial conditions were as follows:

a velocity inlet was used with velocity set at 8, 12, 16, 20, and 24 m/s; a steady-state calculation mode was selected; a realizable k - ϵ model combined with a standard wall function correction method was used; the outlet boundary condition was defined as the pressure outlet; other boundary conditions were defined as stationary walls; the SIMPLEC algorithm was chosen; the second-order upwind format was used for the dissociation of equations; skewness correction was set according to computing requirements; every calculation was set to iterate 1000 times before convergence.

3 Results and discussion

3.1 Numerical simulation results

An orthogonal test was used to study the reduction in skin friction achieved by variable ovoid dimples, which was evaluated by the drag coefficient

(C_D). For tests with multiple factors and levels, the key influencing factors were investigated by intuitionistic analysis. Combined with square-difference analysis, the effect of each factor and the best combination were determined.

Numerical simulation test results of the variable ovoid dimples were substituted into the intuitionistic analysis table for analysis (Table 2) (taking a fluid speed of 24 m/s as an example). K_n is the sum of the results C_D at level n for each parameter; k_n is the average of K_n , which is equal to K_n over 3; R is the difference between the maximum and minimum of k_n . The experimental results were then studied by square-difference analysis (Table 3).

The maximal skin friction reduction was about 10% in test 7 (Table 2). Intuitionistic analysis shows that the best level for each design parameter is level 3 for radius r , level 2 for semimajor l , level 3 for depth h , and level 3 for spacing d . The different effects on skin friction reduction were, in order of

Table 2 Intuitionistic analysis table of results from numerical simulation tests

Item	Radius, r (mm)	Semimajor, l	Depth, h (mm)	Spacing, d (mm)	C_D (%)
Test 1	0.6 (1)	1.25 r (1)	0.2 (1)	2.0 (1)	2.78
Test 2	0.6 (1)	1.50 r (2)	0.3 (2)	2.5 (2)	5.05
Test 3	0.6 (1)	0.50 r (3)	0.4 (3)	3.0 (3)	6.71
Test 4	0.7 (2)	1.25 r (1)	0.3 (2)	3.0 (3)	6.85
Test 5	0.7 (2)	1.50 r (2)	0.4 (3)	2.0 (1)	8.00
Test 6	0.7 (2)	0.50 r (3)	0.2 (1)	2.5 (2)	5.13
Test 7	0.8 (3)	1.25 r (1)	0.4 (3)	2.5 (2)	10.19
Test 8	0.8 (3)	1.50 r (2)	0.2 (1)	3.0 (3)	10.14
Test 9	0.8 (3)	0.50 r (3)	0.3 (2)	2.0 (1)	10.14
K_1	14.54	19.82	18.05	20.92	
K_2	19.98	23.19	22.04	20.37	
K_3	30.47	21.98	24.90	23.70	
k_1	4.85	6.61	6.02	6.97	
k_2	6.66	7.73	7.35	6.79	
k_3	10.16	7.33	8.30	7.90	
R	5.31	1.12	2.28	1.11	

Note: n ($n=1, 2, 3$) in bracket for tests 1–9 means level n

Table 3 Square-difference analysis table of results from numerical simulation tests

Source	Sum of squares	Degree of freedom	F value	$F(0.05)$	Result
Radius, r	43.71	2	22.50	19	Significant
Semimajor, l	1.94	2	1	19	
Depth, h	7.89	2	4.06	19	
Spacing, d	2.12	2	1.09	19	
Grand total	55.66	8			

significance, radius r , depth h , semimajor l , and spacing d . Square-difference analysis (Table 3) also shows that the effect of radius r was the most significant.

3.2 Skin friction reduction mechanism

To study the mechanism of reduction of skin friction by the variable ovoid surface, the distribution of velocity vectors, the variation boundary layer thickness, and the distribution of static pressure were examined. Because the maximal reduction in skin friction was in test 7, model 7 with a fluid speed of 24 m/s was taken as an example for analysis.

3.2.1 Internal coherent structure

A velocity vector graph of the variable ovoid dimples along the middle cross section was extracted (Fig. 7). Regions 1 and 2 in Fig. 7 are enlarged in Figs. 8 and 9, respectively, in which low velocity vortices can be observed. The flow direction near the top of the vortices is the same as that of the outside flow but is contrary at the bottom, causing a secondary vortex effect and greatly reducing the skin friction by converting sliding friction to rolling friction.

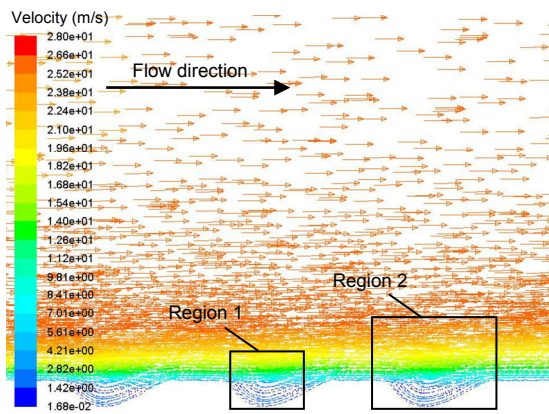


Fig. 7 Velocity vectors of variable ovoid dimples on the middle cross section

A coherent structure of a turbulent boundary layer refers to similar flow features inside the boundary magnitude space. In general, the flow features found in region 1 of Fig. 7 can be considered a coherent structure. The variable ovoid dimples boot the turbulent flow to produce a coherent structure and cause regular disturbance to the turbulent flow.

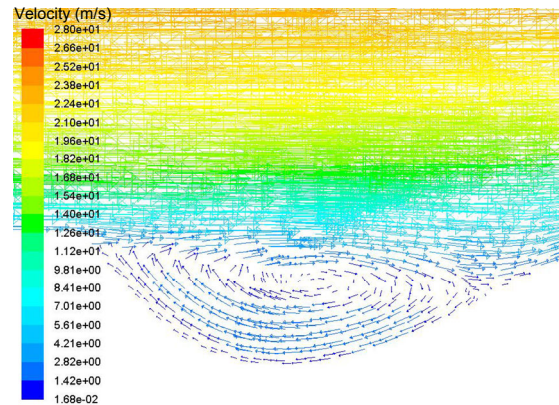


Fig. 8 Enlargement of region 1 in Fig. 7

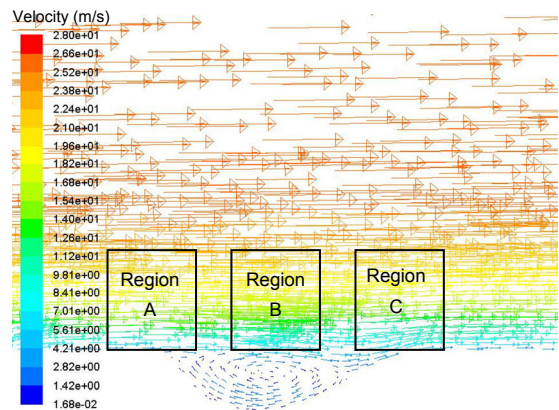


Fig. 9 Enlargement of region 2 in Fig. 7

The details of flow around the vortices are shown in Fig. 9. The flow in region B is clearly stacked. The flow direction changes from a drop to an uptrend in region A, while the direction is opposite in region C. This phenomenon is caused by the absorption function of variable ovoid dimples. When fluid is adsorbed to the near-wall region by variable ovoid dimples, the flow speed is stable and its pulsation is reduced. As a result, the turbulent kinetic energy and turbulent pulsation are decreased.

3.2.2 Variation in boundary layer thickness

The boundary layer is a very thin fluidized bed near the body surface, in which the velocity gradient is so high that the viscous effect is remarkable. However, there is no strict distinction between the boundary layer and the free flow layer in turbulent flow. In general, the thickness of the boundary layer refers to the distance between the body surface and a certain place with a flow speed at 99.5% of the free

flow speed, which can be calculated by the following formula:

$$\delta = \int_0^z \left(1 - \frac{\rho u}{\rho_e u_e} \right) dy, \quad (3)$$

where z is the height of the flow area; ρ and ρ_e are the densities and u and u_e the flow velocities of the free flow and boundary layer, respectively.

Fig. 10 shows the fluid speed along with the height at the middle position 20 mm away from the entrance. The smooth surface has a higher fluid speed than the non-smooth surface, which indicates that variable ovoid dimples have a thicker boundary layer and a smaller velocity gradient. In summary, a variable ovoid surface has two main effects on the boundary layer. Firstly, it increases the boundary layer thickness. Secondly, it reduces the flow velocity gradient near the body surface, resulting in a decrease in energy loss. As a result, the variable ovoid surface has a low resistance effect. Fig. 11 shows the change in boundary layer thickness and drag coefficient with fluid speed. When the fluid speed changes from 8 to 24 m/s, the boundary layer thickness decreases but the drag coefficient increases.

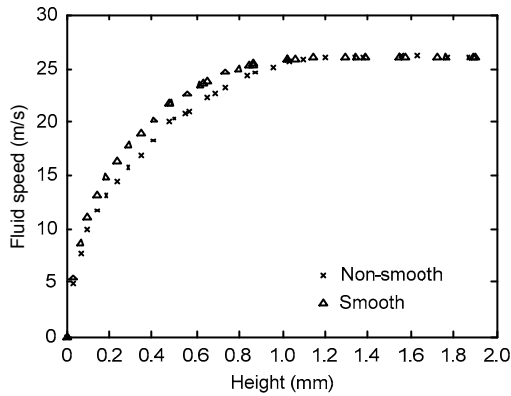


Fig. 10 Variation in fluid speed with the height of the flow area

3.2.3 Effect on pressure

Pressure contours were used to analyze the variation in pressure perpendicular to the direction of flow. The regular variation of static pressure around the variable ovoid dimples is shown in Fig. 12. A single variable ovoid dimple can be divided into windward and leeward regions (Fig. 13). A high

pressure region is formed in the windward region, which contributes to the creation of a low pressure region in the following area. A low pressure region is formed leeward, caused mainly by the lag effect of the previous variable ovoid dimple. Therefore, every variable ovoid dimple produces a knock-on effect on the pressure, and produces regular variation in pressure along the flow direction, which at first changes from low to high and then from high to low.

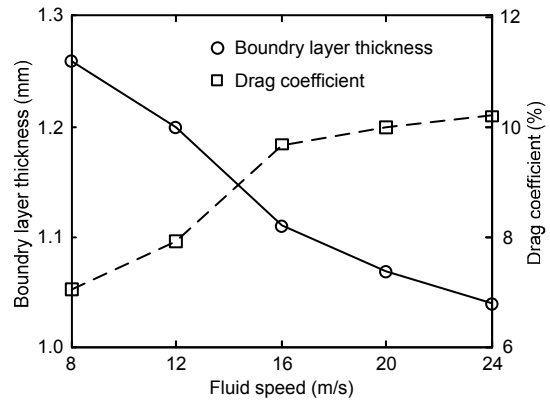


Fig. 11 Variation in boundary layer thickness and drag coefficient with fluid speed

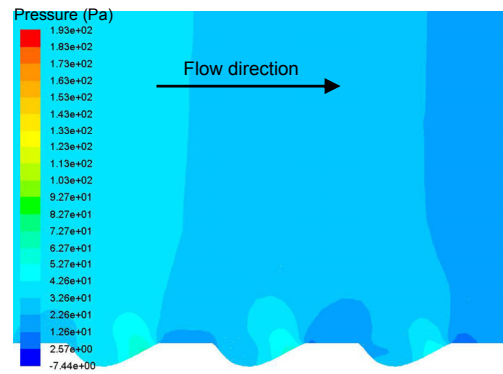


Fig. 12 Pressure contour of variable ovoid dimples on the middle cross section

According to the pressure variation among variable ovoid dimples, the distribution of velocity vertical to the flow direction will change similarly, causing a series of structural variations inside the boundary layer. There are three velocity regions which correspond with the respective pressure distribution regions in the variable ovoid dimples (Fig. 14). The distribution of velocity vertical to the flow direction of a single variable ovoid dimple is shown in Fig. 15, where the three speed regions correspond to the three

respective pressure regions in Fig. 13. Such a velocity distribution plays a positive role in promoting the formation of coherent structures. The pressure gradient between the low speed region and high speed region 1 can promote the forward movement of fluid, which can offset part of the viscous force and reduce the drag.

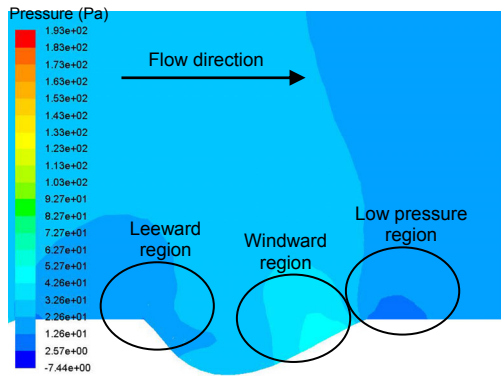


Fig. 13 Pressure contour of a single variable ovoid dimple

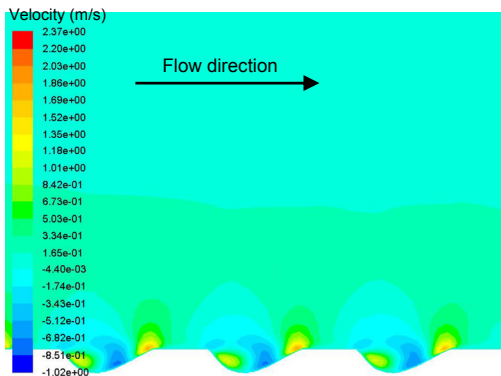


Fig. 14 Velocity contour of variable ovoid dimples on the middle cross section

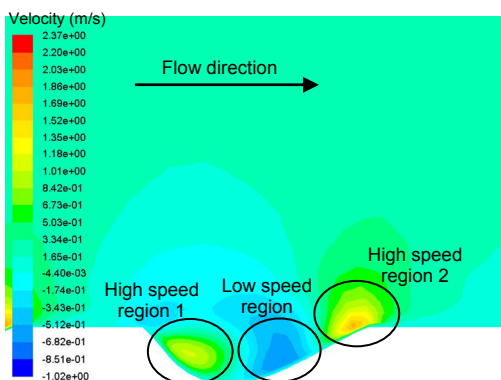


Fig. 15 Velocity contour of a single variable ovoid dimple

4 Conclusions

A variable ovoid non-smooth structure inspired by sand dunes is presented in this paper. Numerical simulation tests found that the structure has a drag reduction effect, reducing drag by 10% at a fluid speed of 24 m/s. Four design parameters affect the skin friction reduction rate. In order of their friction reduction effect, they are radius r , depth h , semimajor l , and spacing d .

Three observations were made in relation to the reduction mechanism of the variable ovoid dimples. Firstly, the coherent structure in variable ovoid dimples causes a regular disturbance to the turbulent flow and adsorption of the fluid at the near-wall region, thereby maintaining the stability of the flow. Secondly, the non-smooth surface can increase the thickness of the boundary layer, which can directly reduce the velocity gradient of the near-wall flow. Thirdly, the variable ovoid dimples have a knock-on effect on the pressure, which changes regularly from low to high and then from high to low along the flow direction. Such a knock-on effect plays a positive role in promoting the formation of coherent structures and reducing the viscous force, leading to skin friction reduction.

This study was limited by the low speed of the air flow. Further investigations should consider high speed or super-high speed air flow. The flow field characteristics of variable ovoid dimples in a water flow also warrant investigation. For research in engineering applications, the variable ovoid dimples could be applied to automobiles or airplanes. There are many methods available to fabricate large-scale non-smooth surfaces, such as non-smooth film coating, bio-replication methods, and 3D printing.

References

- Bixler, G.D., Bhushan, B., 2013. Shark skin inspired low-drag microstructured surfaces in closed channel flow. *Journal of Colloid and Interface Science*, **393**:384-396. <http://dx.doi.org/10.1016/j.jcis.2012.10.061>
- Boiko, A.V., Jung, K.H., Chun, H.H., et al., 2007. Effect of riblets on the streaky structures excited by free stream tip vortices in boundary layer. *Journal of Mechanical Science and Technology*, **21**(1):196-206. <http://dx.doi.org/10.1007/BF03161725>
- Bourisli, R.I., Al-Sahhaf, A.A., 2008. CFD modeling of turbulent boundary layer flow in passive drag-reducing applications. 7th International Conference on Advances

- in Fluid Mechanics, p.79-90.
<http://dx.doi.org/10.2495/AFM080081>
- Bullen, R.D., McKenzie, N.L., 2008. The pelage of bats (Chiroptera) and the presence of aerodynamic riblets: the effect on aerodynamic cleanliness. *Zoology*, **111**(4):279-286.
<http://dx.doi.org/10.1016/j.zool.2007.09.001>
- Choi, J., Jeon, W., Choi, H., 2006. Mechanism of drag reduction by dimples on a sphere. *Physics of Fluids*, **18**(4):041702.
<http://dx.doi.org/10.1063/1.2191848>
- Dean, B., Bhushan, B., 2010. Shark-skin surfaces for fluid-drag reduction in turbulent flow: a review. *Advance in Mechanics*, **368**(1929):4775-4806.
<http://dx.doi.org/10.1098/rsta.2010.0201>
- Dean, B., Bhushan, B., 2012. The effect of riblets in rectangular duct flow. *Applied Surface Science*, **258**(8):3936-3947.
<http://dx.doi.org/10.1016/j.apsusc.2011.12.067>
- Gao, G., Huang, N., 1982. Theoretical and experimental study in stability of the barchan dune vortex flame. *Journal of Engineering Thermophysics*, **3**(1):89-95 (in Chinese).
- Gu, Y.Q., Zhao, G., Liu, H., et al., 2013. Characteristics of drag reduction of bionic dimpled surface of shell rubber ring of aerodynamic extinguishing cannon. *Journal of Jilin University (Engineering and Technology Edition)*, **43**(4):983-990 (in Chinese).
- Kim, J., Choi, H., 2014. Aerodynamics of a golf ball with grooves. *Proceedings of the Institution of Mechanical Engineers, Part P: Journal of Sports Engineering and Technology*, **228**(4):233-241.
<http://dx.doi.org/10.1177/1754337114543860>
- Matthews, J.N.A., 2008. Low-drag suit propels swimmers. *Physics Today*, **61**(8):32-33.
<http://dx.doi.org/10.1063/1.2970208>
- Ren, L.Q., 2009. Progress in the bionic study on anti-adhesion and resistance reduction of terrain machines. *Science in China Series E: Technological Sciences*, **52**(2):273-284.
<http://dx.doi.org/10.1007/s11431-009-0042-3>
- Song, X.W., Zhang, G.G., Wang, Y., et al., 2011. Use of bionic inspired surfaces for aerodynamic drag reduction on motor vehicle body panels. *Journal of Zhejiang University-SCIENCE A (Applied Physics & Engineering)*, **12**(7):543-551.
<http://dx.doi.org/10.1631/jzus.A1000505>
- Viswanath, P.R., 2002. Aircraft viscous drag reduction using riblets. *Progress in Aerospace Sciences*, **38**(6-7):571-600.
[http://dx.doi.org/10.1016/S0376-0421\(02\)00048-9](http://dx.doi.org/10.1016/S0376-0421(02)00048-9)
- Zhang, C.C., Ren, L.Q., Liu, Q.P., et al., 2008. Experimental study on bionic dimpled surfaces of bodies of revolution for drag reduction. *Acta Aerodynamica Sinica*, **26**(1):79-84 (in Chinese).
<http://dx.doi.org/10.3969/j.issn.0258-1825.2008.01.015>
- Zhang, D.Y., Luo, Y.H., Li, X., et al., 2011. Numerical simulation and experimental study of drag-reducing surface of a real shark skin. *Journal of Hydrodynamics, Ser. B*, **23**(2):204-211.
[http://dx.doi.org/10.1016/S1001-6058\(10\)60105-9](http://dx.doi.org/10.1016/S1001-6058(10)60105-9)

中文概要

题目: 变异卵圆形凹坑非光滑表面的气动摩擦减阻研究

目的: 仿生非光滑表面具有降低表面摩擦阻力的作用,传统的非光滑结构有沟槽和凹坑等。本文旨在研究变异卵圆形凹坑非光滑表面的气动摩擦减阻特性及其减阻机理。

创新点: 1. 以仿生学理论为基础,提出变异卵圆形凹坑结构模型,突破现有非光滑结构类型的局限; 2. 采用参数构造的方法研究变异卵圆形各构造参数对表面摩擦阻力减阻的影响。

方法: 1. 采用半径、半轴和坑深 3 个尺寸参数对变异卵圆形凹坑结构进行几何定义,并将非光滑结构以一定纵向间距按矩形排布布置在仿真模型底部; 2. 以 3 个尺寸参数和纵向间距设计“三水平四因素”正交实验,在不同气流流速下进行数值模拟仿真; 3. 通过速度矢量、边界层厚度变化和压力分布研究变异卵圆形凹坑非光滑表面的气动摩擦减阻机理。

结论: 1. 变异卵圆形非光滑表面具有一定的气动摩擦减阻效果,和光滑表面相比,在空气来流速度为 24 m/s 时,有 10%的减阻效果; 2. 正交实验分析表明,4 个试验因素对减阻效果的影响从大到小排列分别为:半径、坑深、半轴和纵向间距; 3. 变异卵圆形凹坑表面增加了边界层的厚度,降低了近壁面区域的速度梯度,减少了剪切力,从而起到了减少摩擦阻力的效果。

关键词: 变异卵圆形凹坑; 非光滑表面; 数值模拟; 表面摩擦减阻